Chemical Engineering Research and Design 205 (2024) 822–829

Contents lists available at ScienceDirect

Chemical Engineering Research and Design

journal homepage: www.elsevier.com/locate/cherd

Local analysis of micro mixing for the Villermaux-Dushman protocol by using the imaging UV-Vis spectroscopy

Torben Frey [a], Felix Kexel [a], Markus Grabellus [b,c], Xuan My Le [a], Marko Hoffmann [a,*], Frank Herbstritt [c], Marcus Grünewald [b], Michael Schlüter [a]

[a] Institute of Multiphase Flows, Hamburg University of Technology, Eissendorfer Strasse 38, Hamburg 21075, Germany
[b] Laboratory of Fluid Separations, Ruhr-University Bochum, Universitaetsstrasse 150, Bochum 44801, Germany
[c] Ehrfeld Mikrotechnik GmbH, Mikro-Forum-Ring 1, Wendelsheim 55234, Germany

ARTICLE INFO

Keywords:
Micro mixing
Imaging UV-Vis spectroscopy
Reactive mixing
Villermaux-Dushman protocol
Incorporation model

ABSTRACT

The Villermaux-Dushman protocol with UV-Vis analytics is an established tool to characterize the global micro mixing performance in process equipment. The local mixing process is described by a micro mixing model (incorporation model), originally designed for turbulent flows. The novel imaging UV-Vis spectroscopy used in this work uncovers locally resolved micro mixing phenomena in a laminar split-and-recombine (SAR) mixer unit manufactured from selective laser-induced etching (SLE). The local absorbance is recorded with a high spatial resolution camera through a telecentric lens and post-processed into local concentration fields of components. The method unveils discrepancies of the micro mixing time determined from the conventional incorporation model in laminar flow and the locally recorded mixing process. The micro mixing time rather needs to be seen as a mean micro mixing time instead. Furthermore, the spatial information obtained by the imaging UV-Vis spectroscopy gives insight into local micro mixing and selectivity, yielding new approaches to equipment optimization.

1. Introduction

The field of micro fluidics is rapidly expanding with the emergence of new manufacturing techniques, high computational resources and new analytical systems. The latter hold great importance when characterizing mixing performance and the capability to reduce fouling in competitive reaction systems. Static milli and micro mixers are an effective tool in continuous polymerization processes to reduce and prevent fouling due to fast micro mixing, as shown for example by Bayer et al. (2000). The mixing performance directly influences efficiency, conversion, and selectivity of a chemical reaction, as shown for example in polymerization (Hungenberg and Wulkow, 2018) or gas-liquid reactions (Kexel et al. 2022). Chemical test reactions help estimate the micro mixing time scale, derived from the known chemical time scale of the limiting reagent (Rodermund et al. 2011; Hoffmann et al. 2006; Reckamp et al. 2017; Guichardon et al. 2000; Falk and Commenge, 2009).

Optical analysis systems are a common way to quantify micro mixing characteristics. UV-Vis spectroscopy is among the established techniques to measure educt or product concentrations (Aubin et al. 2010). The above mentioned methods require at least one optically detectable species (i.e., absorbing or fluorescent properties), such as the Villermaux-Dushman protocol developed by (Fournier et al. 1996). The selectivity achieved by mixing equipment is related to micro mixing times, based on specific micro mixing models. The models are originally developed for turbulent mixing processes, however, due to the lack of models for laminar flow (e.g., in micro mixing equipment) the models are often applied to laminar (static) mixers as well (Liu and Lee, 1999; Fang and Lee, 2001; Rahimi et al. 2017; Kashid et al. 2011; Su et al. 2011).

The novel imaging UV-Vis spectroscopy (Kexel et al. 2021; Frey et al. 2022) used in this work is able to simultaneously detect the local absorbance of multiple species in a transparent flow domain and consequently creates a selectivity or micro mixing map of the domain.

Abbreviations: FVT, Laboratory of fluid separations RUB; IMS, Institute of multiphase flows TUHH; ODE, Ordinary differential equation; RUB, Ruhr-University Bochum; SAR, Split-and-recombine; SLE, Selective laser-induced etching; TRIS, Trishydroxymethylaminomethane; TUHH, Hamburg University of Technology; UV-Vis, Ultra violet and visible light.

* Corresponding author.
E-mail address: marko.hoffmann@tuhh.de (M. Hoffmann).

https://doi.org/10.1016/j.cherd.2024.04.049
Received 30 November 2023; Received in revised form 29 March 2024; Accepted 23 April 2024
Available online 29 April 2024
0263-8762/© 2024 The Author(s). Published by Elsevier Ltd on behalf of Institution of Chemical Engineers. This is an open access article under the CC BY license (http://creativecommons.org/licenses/by/4.0/).

The local analysis of micro mixing is used to assess the validity of micro mixing models in laminar flow applications and the meaning of the derived micro mixing time.

1.1. Villermaux-Dushman protocol

The Villermaux-Dushman protocol consists of two competitive-parallel reactions with differing (by orders of magnitude, depending on the acid concentration) reaction rates. When perfectly mixed, the fast reaction is preferred. The selectivity shifts towards the slow reaction as the reagents of the fast reaction are locally in sub-stoichiometric supply if micro mixing is incomplete. The selectivity therefore yields a quantitative metric of the micro mixing efficiency.

Since the establishment of the protocol, different reaction systems have been developed. This work utilizes the reaction system first documented by Arian and Pauer (2022). The quasi-instantaneous reaction

$$H^+ + (CH_2OH)_3CNH_2 \rightleftharpoons (CH_2OH)_3CNH_3^+ \tag{1}$$

converts fully dissociated perchloric acid ($HClO_4$) using TRIS buffer solution ($(CH_2OH)_3CNH_2$) in an acid-base neutralization reaction. The second slower reaction, i.e., the Dushman reaction

$$6H^+ + 5I^- + IO_3^- \rightarrow 3I_2 + 3H_2O \tag{2}$$

is known as the iodide-iodate reaction and occurs only if reaction (1) is limited by slow micro mixing. It is, however, fast enough to occur before full global mixing is achieved. Reaction (2) produces iodine (I_2), which in turn forms an equilibrium

$$I_2 + I^- \rightleftharpoons I_3^- \tag{3}$$

with triiodide (I_3^-). Arian and Pauer (2021b) describe the detailed kinetics of the reaction system (1) to (3), which are consequently used for the incorporation model in this work. Triiodide shows two characteristic peaks in the UV spectrum, namely at the wavelengths $\lambda_1 = 287$ nm and $\lambda_2 = 353$ nm. The triiodide yield $Y_{I_3^-}$ is typically determined from UV-Vis spectroscopy and, together with the stoichiometric yield at completely segregated conditions

$$Y_{I_3^-,ST} = \frac{6\dot{n}_{IO_3^-,0}}{6\dot{n}_{IO_3^-,0} + \dot{n}_{TRIS,0}} \tag{4}$$

give the segregation index

$$X_s = \frac{Y_{I_3^-}}{Y_{I_3^-,ST}} \tag{5}$$

as a measure of the micro mixing efficiency of the respective equipment and operating conditions. $\dot{n}_{i,0}$ denotes initial condition of the molar flux of species *i*. $X_s = 0$ indicates ideally mixed conditions, and $X_s = 1$ is defined as completely segregated conditions.

1.2. Micro mixing models

In literature, micro mixing is described as mass exchange between fluid elements (Harada et al. 1962), the mixing below the viscous-convective subrange (Bałdyga and Bourne, 1984), or simply diffusive mixing (Kockmann, 2008). The computational effort for resolving the necessary length and time scales is enormous and is often simplified into a set of ordinary differential equations (ODEs). The general governing equation of the established micro mixing models

$$\frac{\partial c_i}{\partial \dot{V}_r} = M(\bar{c}_i - c_i) - R_i \tag{6}$$

describes the change of the reagent's concentration c_i in the reacting volume flow $\dot{V}_r$ as a general mass transport equation with a modeling parameter M and the consumption rate R_i. The parameter M is modeled based on flow characteristics.

The lamellar model (Ottino et al. 1979) defines a surface area S between lamellae depending on molecular diffusion, local stretching, and convection as shown in Fig. 1 (A), whereas the engulfment model (Bałdyga and Bourne, 1984) define the deformation and decay of rotating lamellae dependent on the vorticity ω of the flow field (Fig. 1 (B)).

The incorporation model (Fournier et al. 1996) gives a generalized approach for the problem. As shown in Fig. 1 (C), the growth of the reacting volume $\dot{V}_r$ occurs governed by an incorporation function, instead of a mechanistic model. Due to its simplicity yet good accuracy, the incorporation model is often used for the characterization of mixing equipment with the Villermaux-Dushman protocol. The incorporation model, although assuming turbulent flow conditions, is often used in laminar flows as well since it yields a comparable micro mixing time based on the chemical reaction's selectivity.

2. Material and methods

This work investigates the well-established incorporation model for the micro mixing time determination of static milli mixer in laminar flows. Therefore, the Villermaux-Dushman protocol (1) - (3) is utilized together with an in-line UV-Vis measurement. Additionally, the imaging UV-Vis spectroscopy is applied to determine the local selectivity of the reaction system within the mixer unit.

2.1. Experimental setup

The experimental setup at the Hamburg University of Technology (TUHH, IMS) is presented in Fig. 2. The acidic solution (conc. $HClO_4$, Carl Roth, CAS 76–90–3) is diluted to obtain concentrations between $0.2\ M < c_{H^+} < 0.4\ M$. Full dissociation is assumed for perchloric acid as

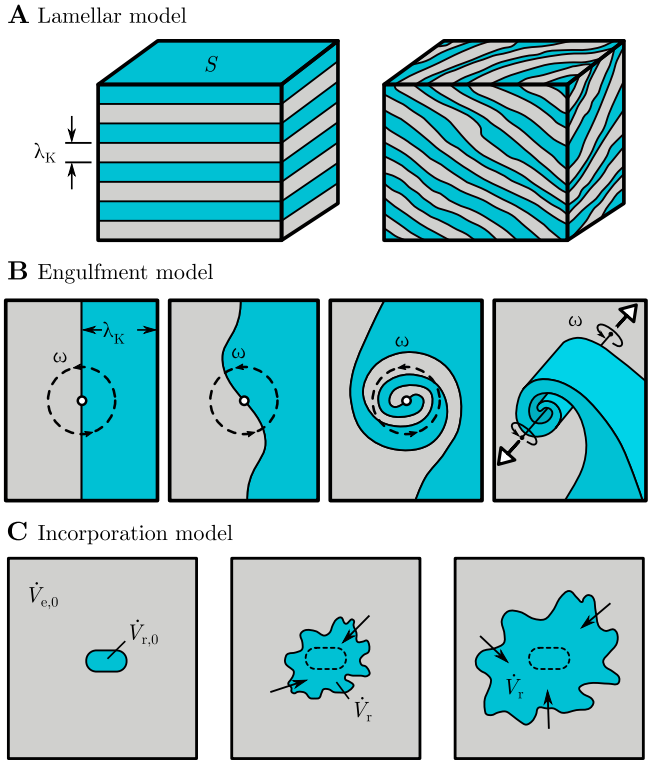

Fig. 1. Common micro mixing models in turbulent flows. (A) Lamellar model with lamella contact surface *S*, according to Ottino et al. (1979); (B) Engulfment model using vortex rotation ω to describe interfacial areas, according to Bałdyga and Bourne (1984); (C) Incorporation model with generalized description of reacting volume growth, according to Fournier et al. (1996).

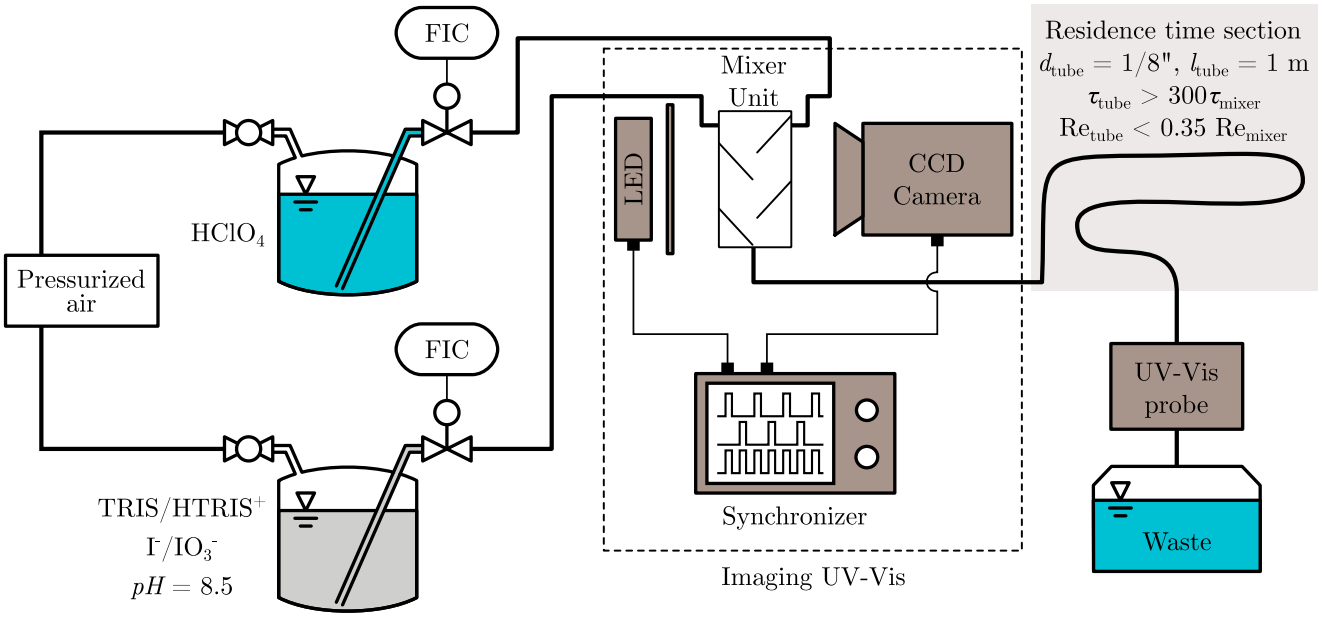

Fig. 2. PID schematic of experimental setup: Acidic and buffer solutions are conveyed pulsation-free by pressurized air to the mixer unit. Imaging UV-Vis spectroscopy records local transmission of LED light through fused-silica mixer to determine local triiodide formation. In-line UV-Vis probe records global triiodide concentration after full equilibrium.

a strong acid. The buffer solution is prepared in a basic environment ($pH = 8.5$) to avoid premature formation of triiodide: TRIS (≥ 99.9 %, Carl Roth, CAS 77–86–1), potassium iodide (≥ 99 %, Carl Roth, CAS 7681–11–0), and potassium iodate (≥ 99.4 %, Carl Roth, CAS 7758–05–6) are solved in aqueous solution. The specific operating conditions are given in Table 1.

Both solutions are conveyed pulsation-free by means of pressurized air in pressure vessels (Thielman UCON GmbH) and the mass flow is controlled by Coriolis flow controllers (FIC, Bronkhorst Nord GmbH). The mixer unit is manufactured by means of selective laser-induced etching (SLE) from two fused silica half shells, representing the geometry of the "Cascade mixer 15" by Ehrfeld Mikrotechnik GmbH. The mixer unit has a hydraulic diameter of $d_h = 1.1$ mm, a channel length of $l = 26.4$ mm and acts as static mixer unit according to the split-and-recombine (SAR) principle.

The imaging UV-Vis spectroscopy is an in-house developed analysis system (Kexel et al. 2021; Frey et al. 2022) consisting of a LED panel ($\lambda_1 = 278$ nm and $\lambda_2 = 395$ nm), a light diffusor sheet, and a CCD camera (PCO Sensicam qe) with a telecentric lens (Sill Optics Correctal T60/0.12D). The LED panel and the camera are controlled and synchronized by an Arduino Uno micro controller. The camera records the phase-shifted LEDs separately with a frequency of $f = 60Hz$ to determine the local transmission of triiodide in the solution.

An in-line UV-Vis probe (Agilent Technologies Cary 60 UV-Vis) measures the global triiodide concentration after the full equilibrium of the iodine-triiodide reaction (3) is reached, i.e., after a residence time section of approx. 1 m. Additionally, the in-line UV-Vis measurements are duplicated in a similar setup with a stainless steel (off-the-shelf) mixer unit at the Ruhr-University Bochum (FVT). The setup at the FVT furthermore uses stainless steel piping and SyrDos syringe pumps to provide pulsation free flow. Both data are used to determine the micro mixing time with the incorporation model.

Table 1
Initial and operating conditions for experimental setup and incorporation model for the fused silica mixer unit at the IMS[1] and the FVT[2].

Set	c_{HClO_4} / mol/L	$\dot{V}$ / mL/min	Re / –
1	0.020[1,2]	4	77
2	0.020[1,2]	8	154
3	0.025[1,2]	4	77
4	0.025[1,2]	8	154
5	0.025[1,2]	16	309
6	0.030[1],0.035[2]	4	77
7	0.030[1],0.035[2]	8	154
8	0.030[1],0.035[2]	16	309
9	0.040[2]	16	309

2.2. Calibration procedure

The in-line UV-Vis spectrophotometer is calibrated by means of a dilution series of triiodide. The stock solution is prepared with an iodide-iodate ratio of 345:1 in acidic environment to shift the selectivity towards triiodide ($S_{I_3^-} = 99.8$ %). The calibration results are shown in Fig. 3 and yield extinction coefficients well in line with literature (Awtrey and Connick, 1951; Wei et al. 2005) at a wavelength of $\lambda = 353$ nm with $R^2 = 0.94$. The much higher absorption at $\lambda = 287$ nm is likely attributed to the optical properties of the flow cuvette (PMMA,

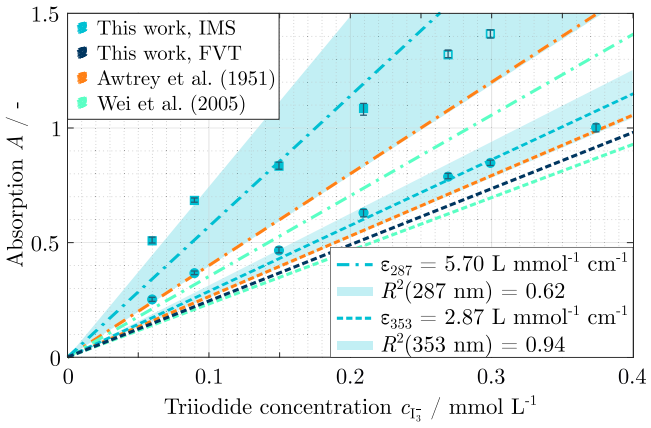

Fig. 3. Experimental calibration of in-line UV-Vis spectrophotometer for $\lambda_1 = 287$ nm and $\lambda_2 = 353$ nm with linear regression at the IMS and comparison to FVT, literature values from Awtrey and Connick (1951) and Wei et al. (2005), exemplarily shown for an optical depth of 10 mm.

rated for $\lambda > 300$ nm) and the increasing measurement uncertainty at large absorbance A. Therefore, it is not used due to the unreliable $R^2 = 0.62$.

The calibration procedure of the imaging UV-Vis spectroscopy requires locally resolved baseline images with light intensity $I_{\lambda,0}(x)$ and maximum attenuation $I_{\lambda,\mathrm{cal}}(x)$. The baseline images are recorded with buffer solution only (no triiodide) and with maximum triiodide concentration ($c_{I_3^-,\mathrm{cal}} = 0.748$ mM), respectively. The local attenuation coefficients

$$\mu_\lambda(x) = \varepsilon_\lambda z(x) = \frac{\log\left(\frac{I_{\lambda,0}(x)}{I_{\lambda,\mathrm{cal}}(x)}\right)}{c_{I_3^-,\mathrm{cal}}} \tag{7}$$

are determined, since the mixer unit depth $z(x)$ varies for each position x. Based on the dilution series depicted in Fig. 3, a linear correlation is assumed for the imaging UV-Vis spectroscopy for each position.

2.3. Incorporation model setup

The mathematical description of the exponential incorporation model in continuous flows is derived from Arian and Pauer (2021a). The model defines two volume flows for $\dot{V}_\mathrm{e}(t)$ (educts) and $\dot{V}_\mathrm{r}(t)$ (reaction). The reaction only takes place in $\dot{V}_\mathrm{r}(t)$ which incorporates $\dot{V}_\mathrm{e}(t)$ over time, according to

$$\dot{V}_\mathrm{r}(t) = \dot{V}_{\mathrm{r},0} + \dot{V}_{\mathrm{e},0} \cdot g(t) \tag{8}$$

with the incorporation function $g(t)$. A schematic illustration of the temporal evolution of the volume flows $\dot{V}_\mathrm{r}(t)$ and $\dot{V}_\mathrm{e}(t)$ as well as the molar fluxes $\dot{n}_i(t)$ of the reagents and products is given in Fig. 4. The reacting volume flow $\dot{V}_\mathrm{r}(t)$ is considered fully mixed and the reactions take place instantly.

The incorporation function used in this work corresponds to the exponential incorporation function

$$g(t) = 1 - \exp\left(-\frac{t}{t_\mathrm{end}}\right) \text{and} \tag{9}$$

$$\frac{\mathrm{d}g(t)}{\mathrm{d}t} = \frac{1}{t_\mathrm{end}} \cdot \exp\left(-\frac{t}{t_{end}}\right) \tag{10}$$

given by Arian and Pauer (2021a). According to the system of reactions (1) to (3), the set of ODEs describing the change of molar fluxes $\dot{n}_i$ in the continuous flow mixer amounts to

$$\frac{\mathrm{d}\dot{n}_{\mathrm{H}^+}}{\mathrm{d}t} = -r_{(1)} - 6r_{(2)}, \tag{11}$$

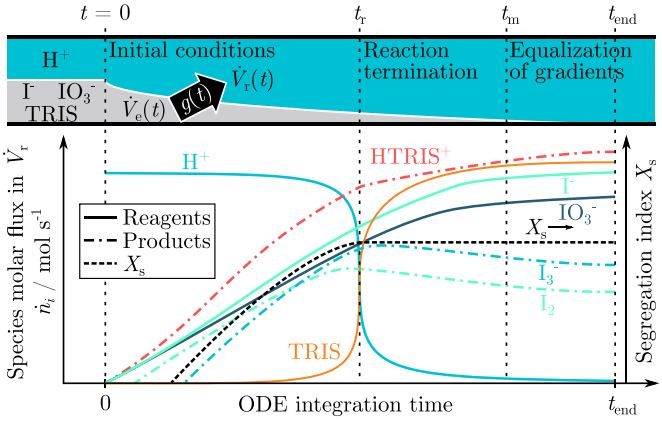

Fig. 4. Incorporation Model: Temporal evolution of volume flows (top) and molar fluxes of species $\dot{n}_i$ in the reacting volume flow $\dot{V}_\mathrm{r}$ on a log-log scale (bottom).

$$\frac{\mathrm{d}\dot{n}_{\mathrm{I}^-}}{\mathrm{d}t} = \dot{n}_{\mathrm{I}^-,0}\frac{\mathrm{d}g(t)}{\mathrm{d}t} - 5r_{(2)} - r_{(3)}, \tag{12}$$

$$\frac{\mathrm{d}\dot{n}_{\mathrm{IO}_3^-}}{\mathrm{d}t} = \dot{n}_{\mathrm{IO}_3^-,0}\frac{\mathrm{d}g(t)}{\mathrm{d}t} - r_{(2)}, \tag{13}$$

$$\frac{\mathrm{d}\dot{n}_{\mathrm{I}_2}}{\mathrm{d}t} = 3r_{(2)} - r_{(3)}, \text{and} \tag{14}$$

$$\frac{\mathrm{d}\dot{n}_{\mathrm{I}_3^-}}{\mathrm{d}t} = r_{(3)} \tag{15}$$

As per definition, the micro mixing time of the incorporation model is $t_\mathrm{m} = t_\mathrm{end}/5$. The ODEs are solved with the MATLAB 2023a solver ode15s for stiff systems with a relative tolerance of 1e-20.

2.4. Initial conditions

The split-and-recombine mixer unit is operated with symmetric flow rate ratios. The initial conditions of the incorporation model correspond to the experimental concentrations and flow rates. The buffer solution is kept at $pH = 8.5$ which is set by adding small amounts of $HClO_4$. The concentrations of the buffer solutions are kept constant for the measurement series at the IMS and the FVT. The buffer solution contains $c_\mathrm{KI} = 31.9$ mM, $c_{\mathrm{KIO_3}} = 6.35$ mM, and $c_\mathrm{TRIS} = 180$ mM. The operating conditions used in this work are shown in Table 1. The hydraulic diameter is defined with the channel volume and wetted contact area, and the Reynolds number is defined with the hydraulic diameter and the mean flow velocity.

3. Determination of the micro mixing time

The incorporation model solves the ODEs (11) - (15) for a defined t_end as boundary condition. Since the time is not known, an iterative process is used to determine t_end and the micro mixing time t_m, respectively. Arian and Pauer (2021a) found two characteristic times, i.e., the reaction time t_r and the micro mixing time t_m. Both times are illustrated in Fig. 4.

The reaction time t_r denotes the point in time where the majority of limiting educts (i.e., H^+) is consumed and the reaction is terminated. t_r is characterized by a sudden drop in acid concentration and the establishment of a constant segregation index plateau X_s (the normalized yield is independent of the further volume flow dilution by $g(t)$). Therefore, by minimizing the squared difference of the globally measured $X_{\mathrm{s,exp}}$ and $X_{\mathrm{s,model}}$ from the incorporation model, the reaction time

$$t_\mathrm{r} := \left|\frac{t_\mathrm{end}}{5}\right|_{\min\left(\left(X_{\mathrm{s,exp}} - X_{\mathrm{s,model}}\right)^2\right)} \tag{16}$$

is obtained.

The micro mixing time t_m is reached when full equalization of gradients is achieved. Since the triiodide concentration in $\dot{V}_\mathrm{r}$ decreases after the reaction termination until $\dot{V}_\mathrm{e}$ is fully incorporated into $\dot{V}_\mathrm{r}$, the micro mixing time

$$t_\mathrm{m} := \left|\frac{t_\mathrm{end}}{5}\right|_{\min\left(\left(c_{I_3^-,\mathrm{exp}} - c_{I_3^-,\mathrm{model}}\right)^2\right)} \tag{17}$$

can be determined by minimizing the squared difference of the triiodide concentration from the experiment and incorporation model. For this purpose, the MATLAB 2023a fminsearch function is used with a tolerance of 1e-20. The ODE solver and the associated functions used in this work are published on Github (Frey, 2023).

4. Results

The results of the experimental measurements are divided into the two analysis methods, i.e., the in-line UV-Vis probe and the imaging UV-Vis spectroscopy. The data recorded by the UV-Vis probe is then used for the determination of micro mixing times with the incorporation model.

4.1. UV-Vis probe measurements

The absorption of triiodide in the solution is consolidated in Table 2 both for the fused silica mixer at the IMS and the stainless-steel mixer at the FVT. In both cases, a residence time section of 1 m length is set up between the mixer and the probe to ensure full equilibrium of the iodine-triiodide reaction (3). The triiodide concentration is determined from the absorption with $\varepsilon_{353,\mathrm{IMS}} = 2.87\ \mathrm{L\ mmol^{-1}cm^{-1}}$ (see Fig. 3) and $\varepsilon_{353,\mathrm{FVT}} = 2.45\ \mathrm{L\ mmol^{-1}cm^{-1}}$, respectively.

For the determination of the segregation index X_s, both the triiodide and iodine concentrations need to be considered. The equilibrium concentrations are determined from the law of mass action. It is noted, that recorded absorbance values $A > 2$ are discarded in this setup. An absorbance of $A = 2$ corresponds to 99% absorption of the incident light and measurement accuracy decreases significantly in this range due to the log-law (7).

4.2. Micro mixing time & incorporation model

The micro mixing times are determined with the incorporation model with exponential incorporation function (8), as defined by Arian and Pauer (2021a). The data basis of the model are both the measurements at the IMS and the FVT (see Table 2). The micro mixing times t_m and the reactions times t_r are depicted in Fig. 5 versus the Reynolds number Re and the total volume flow rate $\dot{V}$, respectively. The micro mixing times at Re = 77 average at $\bar{t}_m(\mathrm{Re} = 77) = 167$ ms and show a relative variance of 20%. With increasing Reynolds number, the micro mixing times decrease to $\bar{t}_m(\mathrm{Re} = 154) = 102$ ms with a relative variance of 27% and $\bar{t}_m(\mathrm{Re} = 309) = 58$ ms with a relative variance 15%. Note, that sets 2 and 5 are excluded from the IMS results, as they are characterized as outliers. The reaction times behave in a similar manner, and are discussed later.

The decrease of micro mixing time with increasing Reynolds number is shown in both experiments. The consistency of the experiments in the fused-silica mixer ($Rq = 0.90$ µm) and the stainless-steel mixer ($Ra = 0.8$ µm) confirms the minor influence of surface roughness and material properties on the flow regimes. However, the fused-silica mixer tends to have slightly larger micro mixing times compared to the smoother surface of the stainless-steel mixer.

The decrease in micro mixing time is expected due to the shift of the flow regime from straight laminar flow (Re < 130) to engulfment flow (130 < Re < 240) and to onset of vortex formation and break-down (Re > 240), as shown by Kockmann (2008) for a T-shaped micro mixer. Similar secondary flow patterns are expected in the SAR mixer unit additionally to the inherent mixing mechanism.

Table 2
Triiodide concentrations determined at wavelength $\lambda = 353$ nm by means of global UV-Vis probe in $HClO_4$/TRIS system after the split-and-recombine mixer unit at the IMS and the FVT.

Set	$c_{I_3^-,\mathrm{IMS}}$	$X_{s,\mathrm{IMS}}$	$c_{I_3^-,\mathrm{FVT}}$	$X_{s,\mathrm{FVT}}$
	mM	%	mM	%
1	0.0140±0.0013	1.02±0.10	0.012±0.000	0.87±0.00
2	0.0162±0.0001	1.18±0.01	0.0069±0.0001	0.50±0.00
3	0.0306±0.0001	1.78±0.00	0.0357±0.0002	2.08±0.01
4	0.0278±0.0001	1.62±0.01	0.0201±0.0002	1.17±0.01
5	0.0285±0.0003	1.66±0.02	0.0167±0.0003	0.97±0.02
6	0.2154±0.0007	9.00±0.03	0.1578±0.0007	6.58±0.03
7	0.1654±0.0014	6.90±0.06	0.0923±0.0005	3.85±0.02
8	0.0780±0.0006	3.25±0.02	0.0752±0.0004	3.13±0.02
9	n/a	n/a	0.134±0.000	4.89±0.01

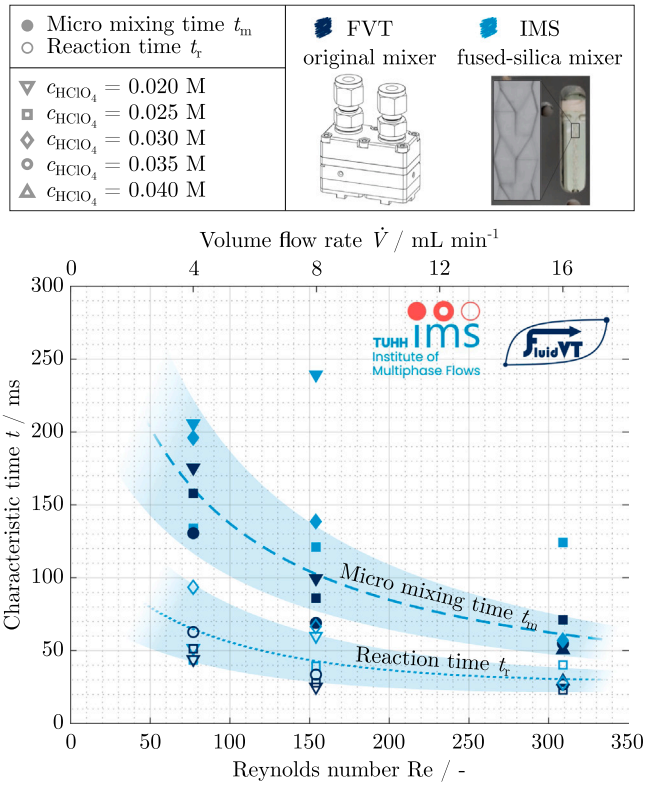

Fig. 5. Micro mixing times and reaction times of the SAR mixer unit at different Reynolds numbers determined from the in-line UV-Vis probe by means of the incorporation model with exponential incorporation function (Arian and Pauer, 2021a).

4.3. Imaging UV-Vis measurements

The imaging UV-Vis spectroscopy gives a local representation of the triiodide concentration fields. The local attenuation coefficients $\mu_\lambda(x)$ are determined from calibration for each LED. Together with the measured intensity $I_\lambda(x)$, the local depth-averaged concentrations

$$c_{I_3^-}(x) = \frac{\log\left(\frac{I_{\lambda,0}(x)}{I_\lambda(x)}\right)}{\mu_\lambda(x)} \tag{18}$$

are returned from the Beer-Lambert law.

The post-processed local triiodide concentration is shown in Fig. 6 versus the mixer unit length l and hydraulic residence time τ. The two feed streams (i.e., acid and buffer solutions) enter the mixer unit from the top and bottom, and are brought together at $\tau = 0$ ms. Triiodide is formed at the contact area ($w = 0$ mm) and no secondary flow patterns are observed before entering the first SAR mixing element ($w = 1.8$ mm). In the following SAR elements, the feed streams are sequentially laminated to form 2^{n+1} laminae, n being the number of SAR elements. At the laminae contact areas, the formation of more triiodide is observed. The increase of triiodide concentration is shown in Fig. 6 both in the contour plot and the SAR element mean concentration.

Due to the low Reynolds number at Re = 77, the laminae are largely unaffected by secondary flow patterns resulting in delayed micro mixing compared to larger Reynolds numbers. The micro mixing time $t_m = 196$ ms at Re = 77 determined from the incorporation model (see Fig. 7) suggests that the equalization of gradients is completed at a hydraulic residence time $\tau = 196$ ms. As depicted in Fig. 6, there are still visible

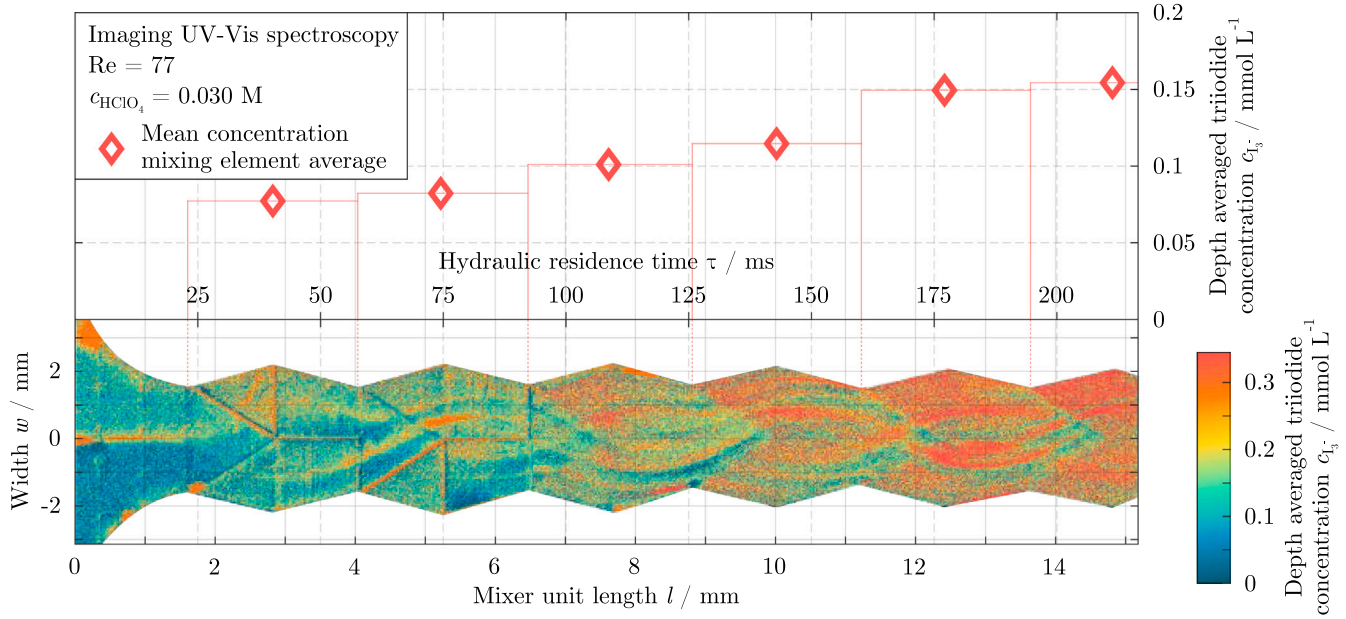

Fig. 6. Imaging UV-Vis: Locally resolved depth averaged triiodide concentration for set 6 (Re = 77, c_{HClO_4} = *0.030* M) in the fused-silica split-and-recombine mixer (bottom) and mean concentration over split-and-recombine elements (top) versus the mixer unit length ***l*** and respective hydraulic residence time τ at Re = *77*.

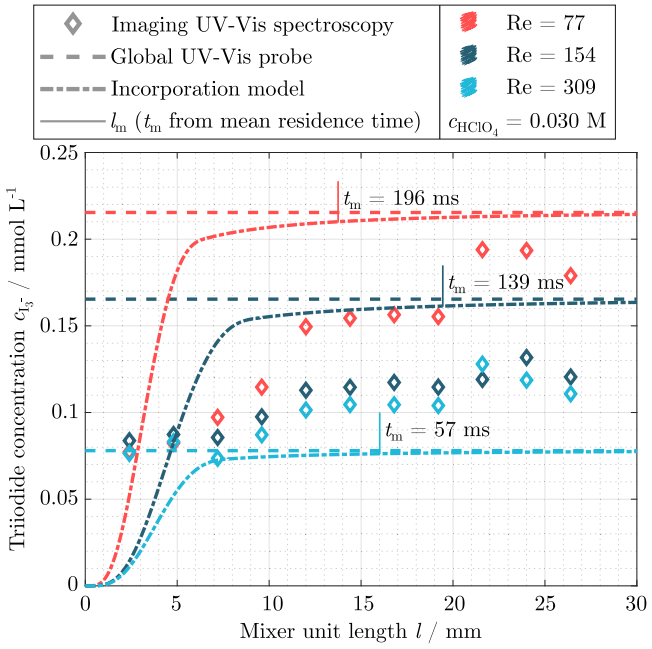

Fig. 7. Spatial resolution of triiodide concentration within the mixer unit at an acid concentration of c_{HClO_4} = *0.030* M and different Reynolds numbers. Comparison of the imaging UV-Vis spectroscopy measurements and the incorporation model converted to mixer length units by means of hydraulic residence time τ.

areas of segregation present at this residence time, showing incomplete mixing.

5. Discussion

The results presented in Section 4 obtained by the global UV-Vis probe and the imaging UV-Vis spectroscopy are compared and discussed concerning their plausibility, accuracy, and significancy for micro mixing characterization.

5.1. Method consistency

Both methods applied in this work are based on transmission spectroscopy. Since both measurements at the IMS are conducted parallelly in the same setup, the measured triiodide concentrations are expected to be consistent. A minor deviation due to the slower equilibrium reaction (3) is however sensible, i.e., the triiodide concentration may be lower at small residence times in the imaging UV-Vis spectroscopy.

The resulting triiodide concentrations determined by means of the UV-Vis probe $c_{I_3^-,global}$ and of the imaging UV-Vis spectroscopy $c_{I_3^-,local}$ (average of last 3 mixer unit elements) are compared in Table 3 for sets 6, 7, and 8. Concerning set 6 and 7, the imaging UV-Vis method shows deviations of 13.4 and 33.4% below the global UV-Vis probe results, respectively. The magnitude of triiodide concentration is smaller directly within the mixer unit, as the full conversion to equilibrium of iodine to triiodide is reached only later in the flow capillary which is captured by the global UV-Vis probe, especially at smaller residence times (i.e., the larger deviation at Re = 154). The data for Re = 77 and Re = 154 is therefore consistent in both measurement methods.

The results recorded at Re = 309 however show larger magnitudes than recorded by the UV-Vis probe. This is not expected and shows a weakness of the imaging UV-Vis spectroscopy method. Assumably, the lower detection limit of triiodide by the imaging UV-Vis spectroscopy (with the camera and LED panel setup in this work) lies around $c_{I_3^-}$ = 0.075 mmol/L, as is evident from Fig. 7. Therefore, the results need to be used with caution when working with low triiodide concentrations. The sensitivity may be improved in future work.

Table 3
Comparison of triiodide concentrations from the global UV-Vis probe and depth averaged triiodide concentration from the imaging UV-Vis spectroscopy at the end of the fused-silica mixer unit at the IMS.

Set	c_{HClO_4}	Re	$c_{I_3^-,global}$	$c_{I_3^-,local}$	Δc_{rel}
	mol/L	–	**mM**	**mM**	%
6	0.030	77	0.2154	0.189	13.4
7	0.030	154	0.1654	0.124	33.4
8	0.030	309	0.0780	0.119	-34.5

5.2. Incorporation model in laminar flow

The application of the incorporation model (for turbulent mixing) to a continuously operated mixer unit in laminar flow conditions might seem unsuitable. However, besides the established application in industry, there is a profound reason to do so. The usage of the selectivity to determine the mixing performance of equipment directly links micro mixing to a competitive chemical reaction. Other research groups show meaningful results for the characterization and comparison of laminar micro mixer (Liu and Lee, 1999; Fang and Lee, 2001; Rahimi et al. 2017; Kashid et al. 2011; Su et al. 2011).

The applicability and meaning of the obtained micro mixing times however require more context. The incorporation model yields micro mixing times t_m and respective micro mixing lengths l_m, when converting the timescale to a length scale using the hydraulic residence time of the mixer unit. The thus obtained spatial progress of the triiodide concentration is plotted in Fig. 7 related to the entire volume flow together with the globally measured concentration by the UV-Vis probe. Additionally, the mean of the depth averaged triiodide concentration over the mixer SAR elements (as described by Fig. 6) determined by the imaging UV-Vis spectroscopy is shown as a reference.

When interpreting the progress of the reaction, the incorporation model clearly underestimates the local micro mixing time or the mixing length, respectively. For example, at $Re = 77$ the reaction terminates at a mixer unit length of $l_r = 6.6$ mm and micro mixing is complete at $l_m = 13.8$ mm. In contrast, the typical flattening of the triiodide concentration (indicating reaction termination) measured with the local imaging UV-Vis spectroscopy occurs at a significantly larger mixer length $l > 15$ mm. This trend is observed for $Re = 154$ as well. The local concentration distributions in Fig. 6 and Fig. 7 underline the observed differences.

The root of the deviations lies in the incorporation model assumptions. Based on the experimentally determined selectivity, the incorporation model finds the closest fit of the boundary conditions of the incorporation function $g(t)$. The function itself assumes an exponential growth of the reacting volume, in which the reaction can instantaneously take place. The slower reaction occurs only, if the educts of the fast reaction are consumed faster than the micro mixing can supply new educt. However, the model assumption also implies the complete presence of the educt of the slow reaction in $\dot{V}_r$. This assumption is valid for continuously stirred tank vessels, the first application of the incorporation model.

In the SAR mixer unit at low Reynolds numbers, the apparent incorporation of the reaction volume is driven by the sequential lamination of the educt feed streams, and subsequently by diffusion. Here, the reacting volume flow $\dot{V}_r$ essentially is described by the lamellae thickness which can be seen as lamellae of triiodide concentration in Fig. 6. The educt of the slow reaction is not in fully contact with the reacting volume flow, as assumed by the incorporation model. To reflect these phenomena, other micro mixing models might be more suitable (e.g., engulfment model, IEM model).

The micro mixing time determined from the incorporation model thus does not represent the global micro mixing time as it does in a turbulent stirred tank. Moreover, the micro mixing time varies locally within the mixer, e.g., in the initial SAR element $n = 1$, the micro mixing time is larger, further downstream of the mixer (and the formation of 2^{n+1} lamellae) the local micro mixing is smaller. If applied to continuous laminar flow applications, the incorporation model rather gives a mean micro mixing time, instead of a uniform global micro mixing time. The mean micro mixing time results in a comparable selectivity to the one of stirred tanks with the same global micro mixing time.

6. Conclusion

This work presents a novel locally resolved transmission spectroscopy analysis method, namely the imaging UV-Vis spectroscopy. The method is compared to a conventional approach of characterizing micro mixing equipment with the incorporation model. Both methods are applied to the Villermaux-Dushman protocol, yielding the temporally (and spatially) resolved reaction progress which allows insights into the phenomenon of micro mixing.

While the incorporation model is originally developed as a description of micro mixing in turbulent stirred tanks, it is able to characterize micro mixing in continuous laminar flow applications, and allows for predictions of selective reaction performance as well. Combined with the Villermaux-Dushman protocol (Perchloric acid, TRIS buffer), the incorporation model gives robust and reproducible mean micro mixing time in a passive split-and-recombine mixer ("Cascade mixer 15" by Ehrfeld Mikrotechnik GmbH) in laminar flow conditions. The effect of surface roughness due to the manufacturing process and material is found to be negligible in the investigated flow conditions ($77 > Re > 309$). The limits of possible operating conditions are imposed by measurement range of the UV-Vis spectrophotometer, since large absorbances $A > 2$ drastically decrease accuracy.

The imaging UV-Vis spectroscopy unveils the 2D-spatial distribution of selectivity within the mixer unit. With the additional information, the weaknesses of the incorporation model assumptions are displayed in laminar flow conditions. While the selectivity is a global parameter that enables comparability between laminar and turbulent flow applications, the micro mixing time derived from the incorporation model gives a mean value, which might locally deviate.

The method enables the geometric optimization of mixer units with direct linkage to the selectivity of a fast competitive reaction. The current setup shows limits at the lower end of absorbance, and will be improved in future work. Furthermore, an organic test reaction system with a competitive-consecutive reaction scheme will be tested in the setup (i.e., the MNIC-DNIC reactions (Tsai et al. 2015; In-Iam et al. 2019; Specht et al. 2020; Schlüter et al. 2021)) to further test the robustness of the imaging UV-Vis setup and the incorporation model in a fluidic system closer to industry applications.

Funding

This work has partially been funded by the joint research program KoPPonA 2.0 as part of the ENPRO initiative (Grant numbers 03EN2004D, 03EN2004H, 03EN2004I). The project is supported by the Federal Ministry for Economic Affairs and Climate Action on the basis of a decision by the German Bundestag.

CRediT authorship contribution statement

Michael Schlüter: Funding acquisition, Resources, Supervision, Writing – review & editing. **Marcus Grünewald:** Funding acquisition, Resources, Supervision, Writing – review & editing. **Frank Herbstritt:** Conceptualization, Funding acquisition, Resources, Writing – review & editing. **Marko Hoffmann:** Funding acquisition, Project administration, Resources, Supervision, Writing – review & editing. **Xuan My Le:** Data curation, Formal analysis, Visualization. **Markus Grabellus:** Data curation, Formal analysis, Methodology, Software, Writing – review & editing. **Felix Kexel:** Conceptualization, Methodology, Validation, Writing – review & editing. **Torben Frey:** Conceptualization, Data curation, Formal analysis, Investigation, Methodology, Software, Visualization, Writing – original draft, Writing – review & editing.

Declaration of Competing Interest

The authors declare that they have no known competing financial interests or personal relationships that could have appeared to influence the work reported in this paper.

Acknowledgments

The authors gratefully acknowledge the financial support provided by the German Federal Ministry for Economic Affairs and Climate Action (BMWK) for the joint research program KoPPonA 2.0.

References

Arian, Elias, Pauer, Werner, 2021a. A comprehensive investigation of the incorporation model for micromixing time calculation. *Chem. Eng. Res. Des.* 175, S. 296–308. https://doi.org/10.1016/j.cherd.2021.09.010.

Arian, Elias, Pauer, Werner, 2021b. Contributions to the kinetics of the iodide-iodate test reaction for micromixing time calculation with extended incorporation models (S.). : *Chem. Eng. Sci.* 237, 116549. https://doi.org/10.1016/j.ces.2021.116549.

Arian, Elias, Pauer, Werner, 2022. Progress in Buffer Choice for the Villermaux-Dushman Reaction. *Ind. Eng. Chem. Res.* 61 (26), S. 9192–9205. https://doi.org/10.1021/acs.iecr.2c00825.

Aubin, Joëlle, Ferrando, Montse, Jiricny, Vladimir, 2010. Current methods for characterising mixing and flow in microchannels. *Chem. Eng. Sci.* 65 (6), S. 2065–2093. https://doi.org/10.1016/j.ces.2009.12.001.

Awtrey, Alice D., Connick, Robert E., 1951. The Absorption Spectra of I 2, I 3-, I -, IO 3-, S 4 O 6= and S 2 O 3=. Heat of the Reaction I 3- = I 2 + I -. In (S.). J. Am. Chem. Soc. 73 (4), 1842–1843. https://doi.org/10.1021/ja01148a504.

Bałdyga, J., Bourne, J.R., 1984. A fluid mechanical approach to turbulent mixing and chemical reaction. Part II Micromixing in the light of turbulence theory. : *Chem. Eng. Commun.* 28 (4-6), S. 243–258. https://doi.org/10.1080/00986448408940136.

Bayer, Thomas, Pysall, Detlev, Wachsen, Olaf, 2000. Micro mixing effects in continuous radical polymerization. Wolfgang Ehrfeld (Hg.): Microreaction Technology: Industrial Prospects. Springer Berlin Heidelberg, S., Berlin, Heidelberg, pp. 165–170. https://doi.org/10.1007/978-3-642-59738-1_15.

Falk, Laurent, Commenge, Jean-Marc, 2009. Characterization of Mixing and Segragation in Homogeneous Flow Systems (Hg.). In: Volker, Hessel, Albert, Renken, Jaap, C. Schouten, Jun-Ichi, Yoshida (Eds.), Micro Process Engineering. Wiley, S., pp. 147–173. https://doi.org/10.1002/9783527631445.ch6 (Hg.).

Fang, J.Z., Lee, D.J., 2001. Micromixing efficiency in static mixer. : *Chem. Eng. Sci.* 56 (12), S. 3797–3802. https://doi.org/10.1016/S0009-2509(01)00098-7.

Fournier, Marie-Christine, Falk, Laurent, Villermaux, Jacques, 1996. A new parallel competing reaction system for assessing micromixing efficiency—Determination of micromixing time by a simple mixing model (In). Chem. Eng. Sci. 51 (23), 5187–5192. https://doi.org/10.1016/S0009-2509(96)00340-5.

Frey, Torben (2023): Incorporation Model for Villermaux-Dushman protocol in continuous flow applications. DOI: 10.5281/zenodo.10103787.

Frey, Torben, Kexel, Felix, Dittmer, Kayla Reata, Bohne, Sven, Hoffmann, Marko, Trieu, Hoc Khiem, Schlüter, Michael, 2022. A Novel Approach for Visualizing Mixing Phenomena of Reactive Liquid-Liquid Flows in Milli- and Micro-Channels. : *Front. Chem. Eng.* 4 https://doi.org/10.3389/fceng.2022.874019.

Guichardon, Pierrette, Falk, Laurent, Villermaux, Jacques, 2000. Characterisation of micromixing efficiency by the iodide–iodate reaction system. Part II: kinetic study. : *Chem. Eng. Sci.* 55 (19), S. 4245–4253. https://doi.org/10.1016/S0009-2509(00)00069-5.

Harada, Makoto, Arima, Kikuo, Eguchi, Wataru, Nagatu, Shinji, 1962. Micro-Mixing in a Continuous Flow Reactor. Coalescence and Redispersion Models. Mem. Fac. Eng., Kyoto Univ. 24 (4), 431–446. Available under: hdl.handle.net/2433/280538.

Hoffmann, Marko, Schlüter, Michael, Räbiger, Norbert, 2006. Experimental investigation of liquid-liquid mixing in T-shaped micro-mixers using μ-LIF and μ-PIV. In (S.). Chem. Eng. Sci. 61 (9), 2968–2976. https://doi.org/10.1016/j.ces.2005.11.029.

Hungenberg, Klaus-Dieter, Wulkow, Michael, 2018. Reactors for Polymerization Processes (Hg.). In: Hungenberg, Klaus-Dieter, Wulkow, Michael (Eds.), Modeling and Simulation in Polymer Reaction Engineering. A Modular Approach. 1. Auflage. Wiley-VCH, Weinheim, pp. 139–162. https://doi.org/10.1002/9783527685738 (Hg.).

In-Iam, Areenan, Wolf, Markus, Wilfer, Claudia, Schaniel, Dominik, Woike, Theo, Klüfers, Peter, 2019. FeNO7 -Type Halogenido Nitrosyl Ferrates: Syntheses, Bonding, and Photoinduced Linkage Isomerism (In). Chem. (Weinh. der Bergstr., Ger.) 25 (5), 1304–1325. https://doi.org/10.1002/chem.201804565.

Kashid, Madhvanand, Renken, Albert, Kiwi-Minsker, Lioubov, 2011. Mixing efficiency and energy consumption for five generic microchannel designs. : *Chem. Eng. J.* 167 (2-3), S. 436–443. https://doi.org/10.1016/j.cej.2010.09.078.

Kexel, Felix, Kameke, Alexandra von, Oßberger, Martin, Hoffmann, Marko, Klüfers, Peter, Schlüter, Michael, 2021. Bildgebende UV/VIS-Spektroskopie zur Untersuchung des Einflusses der Fluiddynamik auf die Entstehung von Haupt- und Nebenprodukt in schnellen konkurrierenden konsekutiven Gas-Flüssig-Reaktionen. In: Chemie Ingenieur Technik, 93, pp. 297–305. https://doi.org/10.1002/cite.202000159.

Kexel, Felix, Alexandra, V.Kameke, Hoffmann, Marko, Schlüter, Michael, 2022. The influence of fluid dynamics on the selectivity of fast gas-liquid reactions in methanol. In: Chemical Engineering and Processing - Process Intensification, 180, 108650. https://doi.org/10.1016/j.cep.2021.108650.

Kockmann, Norbert, 2008. Transport phenomena in micro process engineering. With 17 tables. Springer (Heat and mass transfer), Berlin, Heidelberg. https://doi.org/10.1007/978-3-540-74618-8.

Liu, C.I., Lee, D.J., 1999. Micromixing effects in a couette flow reactor (S.). : *Chem. Eng. Sci.* 54 (13-14), 2883–2888. https://doi.org/10.1016/S0009-2509(98)00341-8.

Ottino, J.M., Ranz, William E., Macosko, Christopher W., 1979. A lamellar model for analysis of liquid-liquid mixing. : *Chem. Eng. Sci.* 34 (6), S. 877–890. https://doi.org/10.1016/0009-2509(79)85145-3.

Rahimi, Masoud, Azimi, Neda, Parsamogadam, Mohammad Amin, Rahimi, Alireza, Masahy, Mohammad Moein, 2017. Mixing performance of T, Y, and oriented Y-micromixers with spatially arranged outlet channel: evaluation with Villermaux/Dushman test reaction. : *Micro Technol.* 23 (8), S. 3117–3130. https://doi.org/10.1007/s00542-016-3118-6.

Reckamp, Joseph M., Bindels, Ashira, Duffield, Sophie, Liu, Yangmu Chloe, Bradford, Eric, Ricci, Eric, et al., 2017. Mixing Performance Evaluation for Commercially Available Micromixers Using Villermaux-Dushman Reaction Scheme with the Interaction by Exchange with the Mean Model. : *Org. Process Res. Dev.* 21 (6), S. 816–820. https://doi.org/10.1021/acs.oprd.6b00332.

Rodermund, Kathrin, Grünewald, Marcus, Schael, Frank, Herbstritt, Frank, Heck, Joachim, 2011. Microstructured Mixers and Hydrocyclons for Multiphase Contacting and Separation. : *Chem. Ing. Tech.* 83 (7), S. 1036–1043. https://doi.org/10.1002/cite.201100020.

Schlüter, Michael, Kexel, Felix, Kameke, Alexandra von, Hoffmann, Marko, Herres-Pawlis, Sonja, Klüfers, Peter, et al., 2021. Visualization and Quantitative Analysis of Consecutive Reactions in Taylor Bubble Flows (Hg.). In: Dieter Bothe, Michael Schlüter, Herres-Pawlis, Sonja, Ulrich, Nieken (Eds.), Reactive Bubbly Flows, Bd. 128. Springer International Publishing (Fluid Mechanics and Its Applications), Cham, pp. 507–543. https://doi.org/10.1007/978-3-030-72361-3_21 (Hg.).

Specht, Pascal, Oßberger, Martin, Klüfers, Peter, Schindler, Siegfried, 2020. Kinetic studies on the reaction of NO with iron(ii) complexes using low temperature stopped-flow techniques. In (S.). Dalton Trans. (Camb., Engl.: 2003) 49 (27), 9480–9486. https://doi.org/10.1039/D0DT01764G.

Su, Yuanhai, Chen, Guangwen, Yuan, Quan, 2011. Ideal micromixing performance in packed microchannels. : *Chem. Eng. Sci.* 66 (13), S. 2912–2919. https://doi.org/10.1016/j.ces.2011.03.024.

Tsai, Ming-Li, Tsou, Chih-Chin, Liaw, Wen-Feng, 2015. Dinitrosyl iron complexes (DNICs): from biomimetic synthesis and spectroscopic characterization toward unveiling the biological and catalytic roles of DNICs. In: Accounts of chemical research, 48, pp. 1184–1193. https://doi.org/10.1021/ar500459j (S.).

Wei, Yong-Ju, Liu, Cui-Ge, Mo, Li-Ping, 2005. Ultraviolet absorption spectra of iodine, iodide ion and triiodide ion. In: Guang pu xue yu guang pu fen xi = Guang pu, 25, pp. 86–88 (S.).